ISIJ International, Vol. 44 (2004), No. 1, pp. 187–196

Fragmentation of Orientation within Grains of a Cold-rolled Interstitial-free Steel

Mark Denis NAVE and Matthew Robert BARNETT

School of Engineering and Technology, Deakin University, Pigdons Road, Geelong, Vic. 3217 Australia.
E-mail: mnave@deakin.edu.au

(*Received on June 16, 2003; accepted in final form on August 28, 2003*)

The formation of a favourable recrystallization texture in interstitial-free (IF) steels depends on the availability and activation of particular nucleation sites in the deformed microstructure. This paper presents a description of the deformed microstructure of a commercially cold-rolled IF steel, with particular emphasis on the microstructural inhomogeneities and short-range orientational variation that provide suitable nucleation sites during recrystallization. RD-fibre regions deform relatively homogeneously and exhibit little short-range orientational variation. ND-fibre regions are heavily banded and exhibit considerable short-range orientational variation associated with the bands. While the overall orientational spread of ND-fibre grains frequently is about the ND-axis, the short-range orientational variation often involves rotation about axes in the TD–ND plane that are nearer to the TD than the ND.

KEY WORDS: steel; IF steel; cold rolling; texture; misorientation; electron backscatter diffraction; EBSD; shear bands.

1. Introduction

The high formability of cold-rolled and recrystallized interstitial-free (IF) steels is primarily due to a strong $\langle 111\rangle \| \mathrm{ND}$ (ND-fibre or γ-fibre) texture that forms during recrystallization.[1] Both nucleation and growth processes contribute to the development of this texture, although the relative importance of each has been the subject of much debate in the literature.[2–11] Recent work indicates that oriented nucleation is primarily responsible for the development of the ND-fibre texture in IF steels with moderately high cold-rolling reductions (75 to 90%).[2,3,11] Since nucleation occurs primarily in regions of high orientation gradient and high stored energy, oriented nucleation is a natural consequence of the variation of these two parameters with orientation.[3,12–15]

It has been well established that orientation gradients and stored energy levels in cold-rolled steels are higher in ND-fibre grains than RD-fibre grains and this is the primary reason for the ND-fibre annealing texture.[3,12–15] However, even within deformed ND-fibre grains, particular nucleation sites (such as grain boundaries and in-grain shear bands) favour particular orientations of recrystallization nuclei.[5,16,17] Consequently, the availability (or lack of availability) of certain nucleation sites may influence the finer features of the recrystallization texture, such as the shape of the ND-fibre and the locations of the maxima along the fibre.[4] An extreme example of this effect is seen in coarse-grained low-carbon steels, where the relatively abundant nucleation at shear bands results in the formation of a Goss annealing texture.[18]

Detailed investigation of texture development during cold-rolling has led to the conclusion that most ND-fibre grains rotate along the ND-fibre during rolling.[19] This does not necessarily imply that all parts of each grain are rotating uniformly along the ND-fibre, nor that intragranular fragmentation necessarily occurs about the ND-axis. Shear banding in $\{111\}\langle 112\rangle$ grains produces rotations about $\langle 110\rangle \| \mathrm{TD}$.[4,20] However, a tendency for ND-rotation has been reported for misorientations between elongated subgrains in ND-fibre grains[14] and rotations about the ND have been measured near the grain boundaries of ND-fibre grains.[21] Furthermore, fragmentation of ND-fibre grains into regions rotated about the ND, by deformation banding in the RD–TD plane, has been modelled and observed.[6,22]

This paper presents an experimental study of orientational fragmentation in a commercially cold-rolled IF steel, with a particular focus on the fragmentation of grains belonging to the ND-fibre. The fragmentation present in a grain will depend not just upon its approximate orientation but upon a number of other factors, such as the size, shape and orientation history of the grain and also its neighbours. For this reason, there is expected to be significant variation in the degree and type of fragmentation present in grains having a similar orientation as well as some common features. The use of electron back-scatter diffraction (EBSD) to characterize the fragmentation of a considerable number of grains of similar orientation enables the common features of fragmentation behaviour to be substantiated to a degree not possible in many previous studies where the use of transmission electron microscopy (TEM) limited measurements to a small number of grains which often had widely differing orientations.[21,23]

2. Experimental Procedure

Electron backscatter diffraction (EBSD) and forescatter imaging in a field-emission gun scanning electron micro-

scope (FEG-SEM) were used to investigate the microstructural and orientational fragmentation of grains in a commercially cold-rolled (75% reduction) titanium-stabilized interstitial-free steel. The composition of the steel is listed in **Table 1**. The steel was prepared by standard metallographic techniques and the final polishing step was with colloidal silica. Both EBSD mapping and forescatter imaging were conducted using the same microscope settings: an accelerating voltage of 20 kV and a 60 μm aperture. The specimen was positioned at a working distance of 25 mm and at a tilt of 70°. An EBSD map covering a 360×360 μm area (1 200×1 200 pixel array, 0.3 μm pixel spacing) was taken on each of the RD–ND and RD–TD sections. Forescatter images were taken of selected regions within the areas covered by the EBSD maps.

In order to save space when describing the microstructural and orientational characteristics of grains having various orientations (and for convenience of labelling on figures) the nomenclature adopted by Samajdar *et al.*[3] is used. The classification scheme is shown in **Table 2**. Letters represent the main texture components occurring in cold-rolled steel (H, I, E, F) as well as a minor component of interest (designated J in this paper). It may be noted that there is some overlap between the I and E classes, since an orientation was considered to belong to a particular orientation class if it was within 15° of the ideal orientation corresponding to that class. A grain or region was considered to belong to a particular orientation class if the majority of orientations within it belonged to that class. However, when selecting grains or regions belonging to each class for further analysis, preference was given to grains or regions in which a high proportion of orientations were quite close to the ideal orientation for that class. While using this method carries some risk of favouring grains or regions having a lower overall orientational spread, it was felt that this effect was likely to be small and considerably outweighed by the benefit of ensuring that the results are as representative as possible of grains or regions having orientational spreads centred near the relevant ideal orientations.

The thickness (in the normal direction) of ten grains in each of the main orientation classes, H: {001}⟨110⟩, I: {112}⟨110⟩, E: {111}⟨110⟩ and F: {111}⟨112⟩, was measured and a mean thickness was calculated for each class. Misorientation profiles (based on the minimum misorientation angle) were measured on five regions belonging to each main orientation class in each section (RD–ND and RD–TD). Each region selected was contained wholly within a single deformed grain. A 15 μm long line, parallel to the rolling direction, was drawn across each region and the misorientation profile (the misorientation of each pixel in the line with respect to the preceding pixel) was recorded. Hypothesis testing was carried out in order to identify any statistically-significant differences between the misorientation profiles for each orientation class. Misorientations less than 1.5° were excluded from the analysis as it is likely that a significant proportion of these misorientations are within the angular variation of the indexing of EBSD patterns during high-speed mapping.

Orientational change within ND-fibre grains was then investigated in further detail. Two different types of misorientation angle distribution were calculated for each of eight ND-fibre grains (four E grains and four F grains) on each of the RD–ND and RD–TD sections. The first type of distribution calculated for each grain—the uncorrelated distribution—was calculated by taking a random subset consisting of one-fifth of the orientations in the grain and then comparing each orientation in the subset with every other orientation in the subset. The uncorrelated distribution gives a measure of the overall spread of the grain in orientation space. The second type of distribution calculated for each grain—the correlated distribution—was calculated by calculating the misorientations between neighbouring pixels and including in the distribution all misorientations greater than 2°. The correlated distribution provides a measure of the degree of short-range fragmentation within the grain.

While the misorientation angle distributions provide a measure of the magnitude of long-range (uncorrelated) and short-range (correlated) orientational change within each grain, an analysis of the distribution of the misorientation axes is necessary to provide a full picture of the nature of the orientational change. Consequently, distributions of the misorientation axes were calculated for each grain using the two different approaches described above (uncorrelated and correlated) and each of these were plotted as pole figures (with respect to the sample coordinate system) and as inverse pole figures (with respect to the crystal coordinate system). The uncorrelated misorientation axis distributions include misorientation axes for all misorientations greater than 2°, while the correlated misorientation axis distributions include axes for misorientations between 2 and 8°. This choice of angular range is discussed in the results section where the distributions are presented.

Table 1. Composition of the commercially cold-rolled interstitial-free steel.

Fe	C	N	Ti	Mn	S	P	Al
Bal.	0.0025	0.0029	0.084	0.15	0.012	0.009	0.042

Table 2. Orientation classes and their corresponding ideal orientations.

Orientation Class	Ideal Orientation
H	{001}<110>
I	{112}<110>
E	{111}<110>
F	{111}<112>
J	{110}<110>

3. Results

The texture of the steel (as measured on an RD–ND sec-

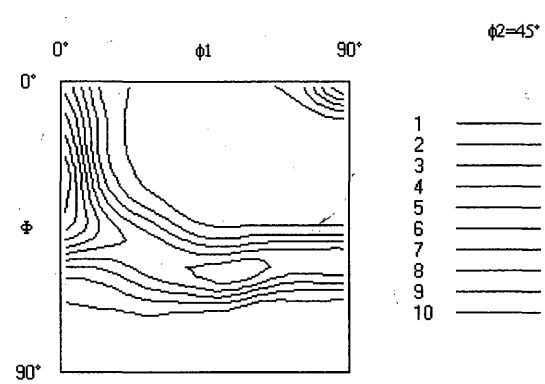

Fig. 1. The texture of the industrially cold-rolled IF steel, illustrated by the φ_2=45° section (Bunge notation) of the ODF. Intensities are expressed in multiples of the intensity given by a random distribution of orientations.

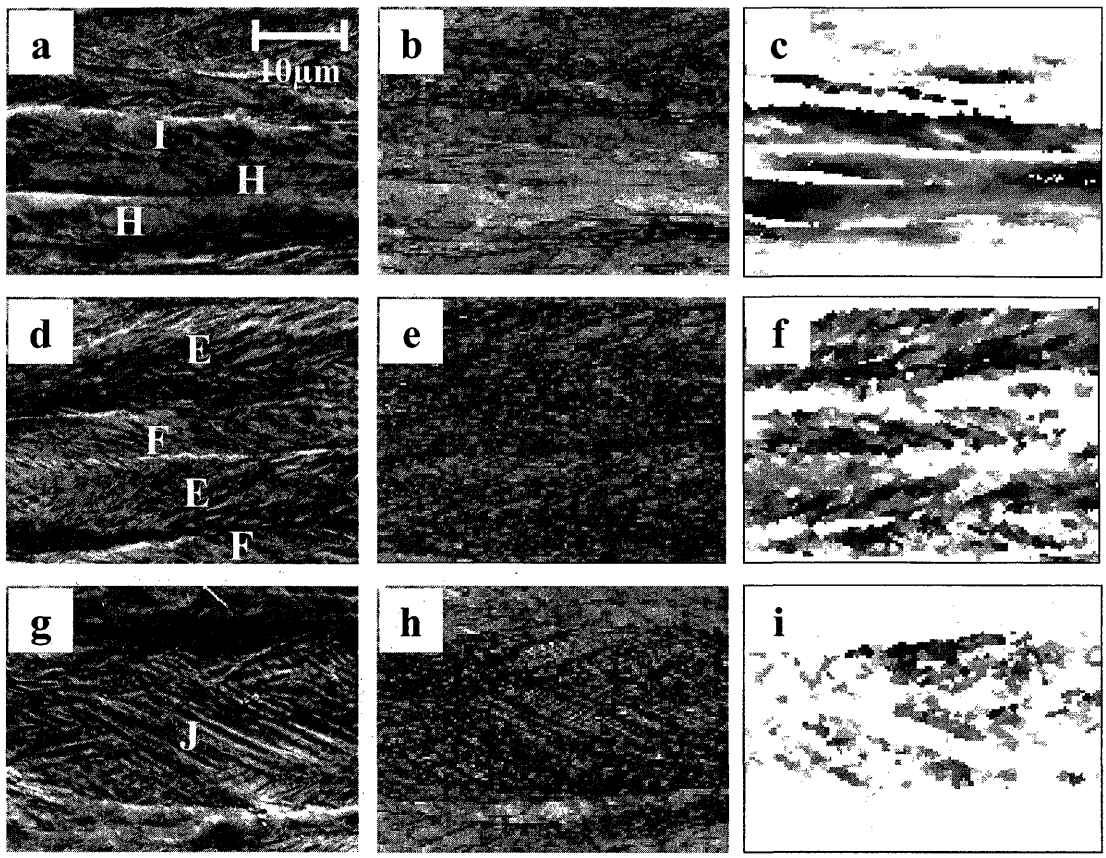

Fig. 2. Parts of the RD–ND section showing (a)–(c) RD-fibre grains with orientations H and I, (d)–(f) ND-fibre grains with orientations E and F, (g)–(i) a grain having mainly J orientation. In the first column (a), (d), (g) are forescatter electron images, in the second column (b), (e), (h) are Kikuchi band contrast images and in the third column (c), (f), (i) are orientation maps showing deviation from the ideal orientations in a grey-scale from black at the ideal orientations to white 15° or more from the ideal orientations.

tion containing approximately 300 to 400 grains) is shown in **Fig. 1**. It is comparable to textures reported in the literature for cold-rolled IF steels of relatively similar composition and rolling reduction.[13,24,25] The density along the RD-fibre increases steadily from 6 at Φ=0°, {001}⟨110⟩, to a peak of 10 at Φ=30°, half-way between {113}⟨110⟩ and {112}⟨110⟩. Beyond Φ=45°, the density decreases rapidly, dropping below 1 at Φ=70°. The density along the ND-fibre is reasonably uniform, varying from 6 or 7 at the {111}⟨110⟩ orientations (φ_1=0° and φ_1=60°) to approximately 5 at the {111}⟨112⟩ orientations (φ_1=30° and φ_1=90°).

The microstructure of the steel is also typical of a cold-rolled steel, with significant differences between RD-fibre grains and ND-fibre grains in their overall shape and internal structure. The RD-fibre grains generally have a much higher aspect ratio on the RD–ND section (*i.e.* are more elongated in the RD and narrower in the ND) compared with the ND-fibre grains. Grains belonging to the RD-fibre orientations, H and I, have a mean thickness in the normal direction of 3.5 μm, while grains belonging to the ND-fibre orientations, E and F, have a mean thickness in the normal direction of 6.8 μm. While the large difference in mean thickness between RD-fibre and ND-fibre grains is statistically significant (at the 95% confidence level using a two-sample *t*-test[26]), there is no significant difference in mean thickness between H and I grains, or between E and F grains (using the same test method and confidence level).

The internal structures of grains belonging to several different orientation classes are shown in **Fig. 2** (RD–ND section) and **Fig. 3** (RD–TD section). The RD-fibre grains (H and I) have relatively little internal structure, while the ND-fibre grains (E and F) are usually marked by a large number of bands. On the RD–ND section, the bands are inclined to the RD, typically by between 20 and 35 degrees. Some ND-fibre grains are marked by a set of (approximately parallel) bands that have the same sense of inclination (positive or negative) with respect to the RD. Some ND-fibre grains (most often E orientations) have sets of positively and negatively inclined bands, giving them a "cross-hatched" appearance. On the RD–TD section, the bands are roughly parallel to the TD in most cases. Grains consisting mainly of J orientation are particularly thick (in the ND) and heavily banded (Figs. 2(g)–2(i), Figs. 3(m)–3(o)). The different degree of banding in the differently oriented grains and the morphology of the bands is revealed well in the forescatter images (left-hand columns of Figs. 2 and 3) and band contrast images (centre columns). The orientation maps (right-hand columns of Figs. 2 and 3) clearly reveal substantial short-range orientational variation associated with the banding in the ND-fibre (E, F) and J grains, in contrast to the relative absence of short-range orientational change in the RD-fibre (H, I) grains, where there the degree of banding is much less.

The higher degree of short-range orientational variation in ND-fibre grains (E, F) compared with RD-fibre grains (H, I) is confirmed and quantified in **Fig. 4**, which shows the distribution, mean and median of misorientations (minimum angle representation) measured parallel to the RD in regions belonging to each orientation class. The mean for each class (Fig. 4(c)) is shown to enable comparison with figures reported in the literature, while the median (Fig.

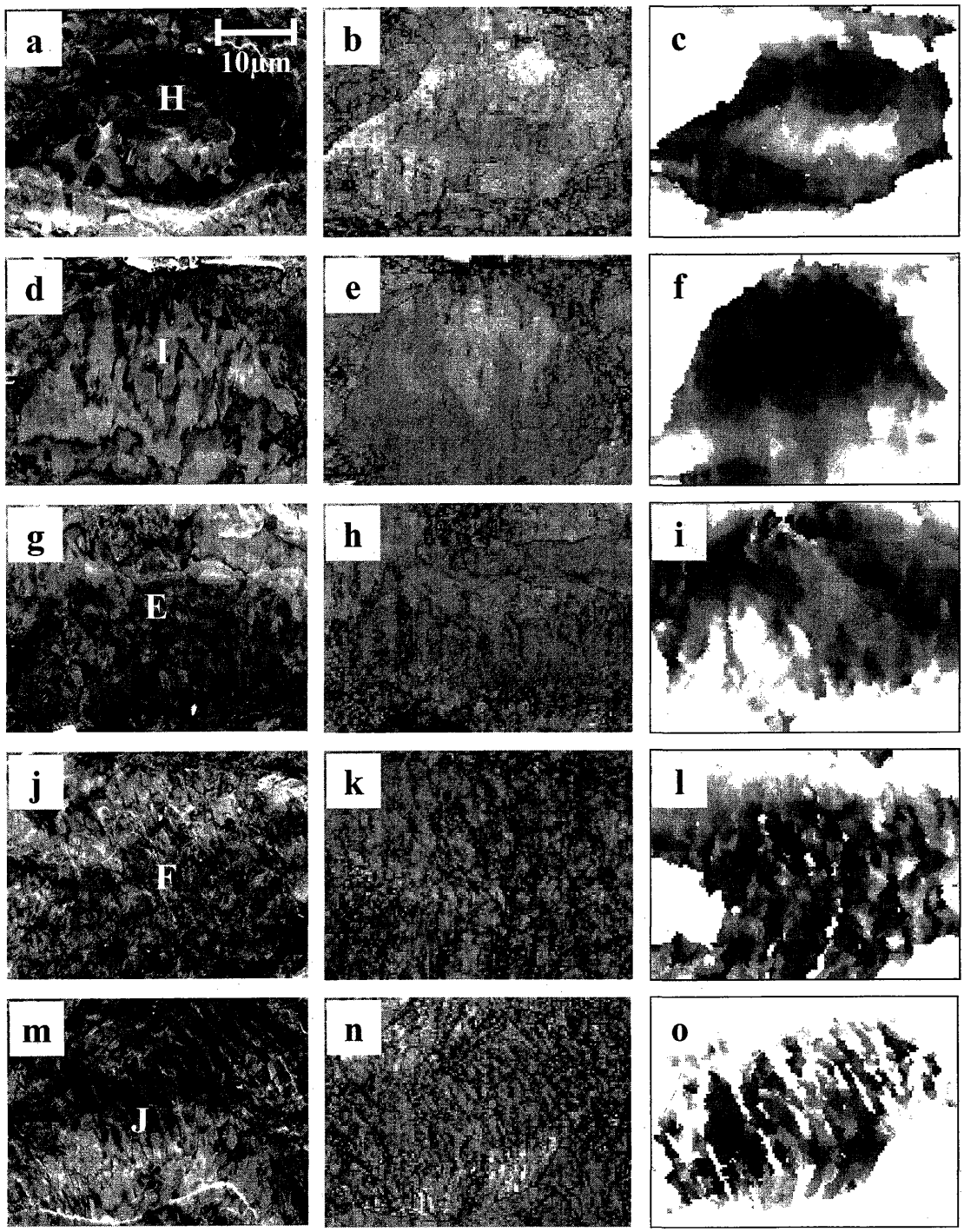

Fig. 3. Parts of the RD–TD section showing (a)–(f) RD-fibre grains with orientations H and I, (g)–(l) ND-fibre grains with orientations E and F, (m)–(o) a grain having mainly J orientation. In the first column (a), (d), (g), (j), (m) are forescatter electron images, in the second column (b), (e), (h), (k), (n) are Kikuchi band contrast images and in the third column (c), (f), (i), (l), (o) are orientation maps showing deviation from the ideal orientations in a grey-scale from black at the ideal orientations to white 15° or more from the ideal orientations.

4(d)) is normally considered a more appropriate measure of highly-skewed distributions such as these (Fig. 4(a)). In this case, the same conclusions are reached whether the *t*-test[26] is used to compare the distribution means or the Mann–Whitney *U*-test[26] is used to compare the ranked distributions: the difference in misorientation distribution between RD-fibre regions and ND-fibre regions is highly significant, while the differences between H and I regions and between E and F regions are not significant at the 95% confidence level.

It should be noted that any measure of average misorientation, while of some use in estimating an average relative stored energy for a region of the deformed microstructure, is of limited benefit in estimating relative nucleation frequencies in different regions as recrystallization nuclei are likely to come from the extreme upper ends of the distributions. For this purpose, a measure of the proportion of misorientations above some critical value may be a more valuable measure. In this context, it is worth noting that RD-fibre regions contain no misorientations greater than 6°, whereas around 10% of the misorientations in ND-fibre regions are greater than 6° (Fig. 4(b)).

Pole figures—{001}, {110}, {111} and {112}—were plotted for each of sixteen ND-fibre grains (four E grains and

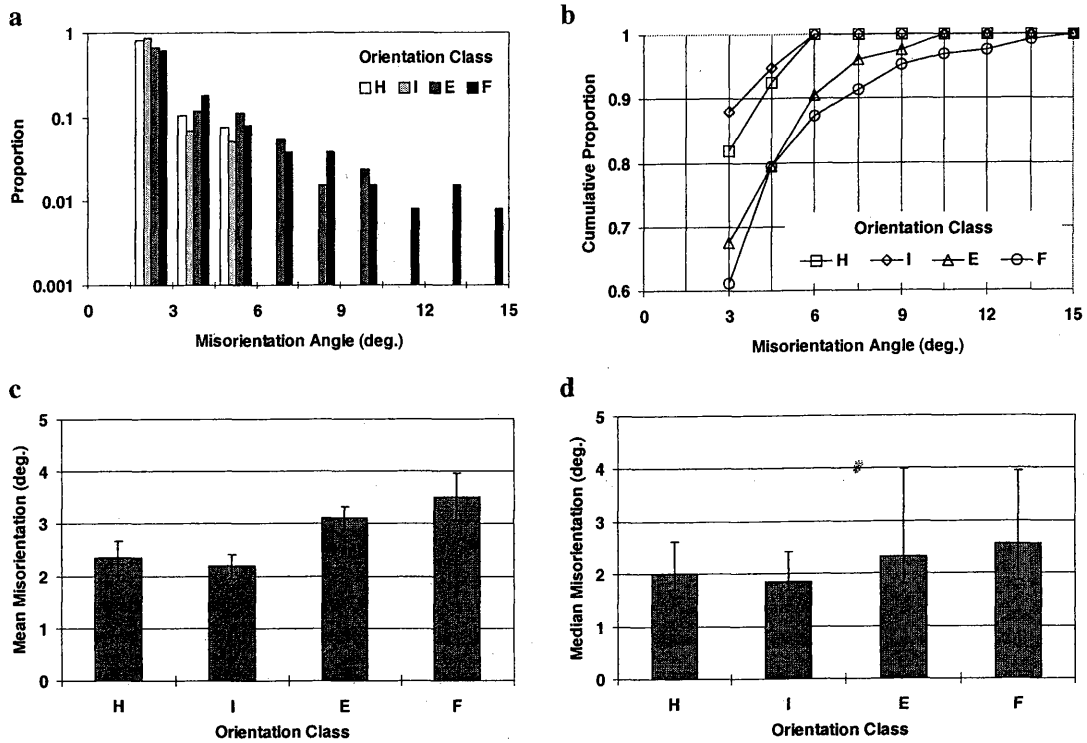

Fig. 4. Distribution of misorientation angles greater than 1.5° between neighbouring pixels in regions belonging to orientation classes H, I, E and F, measured parallel to the RD: (a) relative frequency, (b) cumulative relative frequency, (c) mean with 95% confidence interval and (d) median with lower and upper quartile.

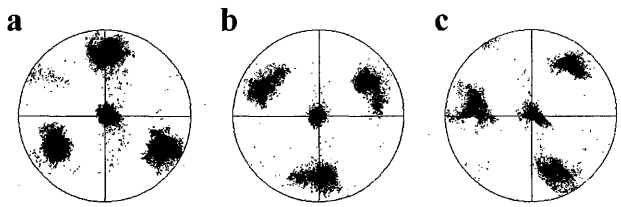

Fig. 5. {111} pole figures for selected ND-fibre grains, showing (a) orientational spread not concentrated about a specific axis, (b) orientational spread concentrated about the ⟨111⟩||ND axis, (c) orientational spread concentrated about a different axis.

four F grains on the RD–ND section and four E grain and four F grains on the RD–TD section) to reveal any consistencies in the overall orientational spreads of the grains. The orientational spreads were classified into three types, which can be conveniently illustrated using {111} pole figures (**Fig. 5**). Grains belonging to the first type (Type A) were spread fairly evenly in all directions about their average orientation (Fig. 5(a)). Grains belonging to the second type (Type B) had an overall orientational spread concentrated about the ⟨111⟩||ND axis (Fig. 5(b)). Grains belonging to the third type (Type C) had an overall orientational spread concentrated about an axis that was not ⟨111⟩||ND (Fig. 5(c)). The nature of the short-range orientational variation in a number of ND-fibre grains was investigated by preparing orientation maps showing angular deviation about three mutually-perpendicular axes (examples are given in **Fig. 6**). However, most grains appeared to show some rotation on the scale of the banding about each of the three axes and it was difficult to ascertain whether a particular rotation axis was preferred.

In order to further quantify the short-range and long-range orientational variation occurring in ND-fibre grains, spatially-correlated and spatially-uncorrelated misorientation angle distributions (**Fig. 7**) and misorientation axis distributions (Figs. 8–12) were calculated for each of the sixteen ND-fibre grains. The spatially-uncorrelated misorientation angle distributions (a measure of the overall orientational spread of a grain) had maxima in the range 6–14°, but tails extending past 30°. In contrast, the spatially-correlated distributions had maxima at very low angles and had very few misorientations greater than 15°. This demonstrates that the long-range orientational variation in ND-fibre grains is much greater in magnitude than the short-range orientational variation. The misorientation angle distributions for E and F grains are very similar, although the correlated distributions (Fig. 7(b)) do suggest that F grains may have slightly less low-angle misorientations and slightly more high-angle misorientations between neighbours, an observation which is consistent with the slightly higher average misorientation in F grains than E grains measured using lines scans parallel to the RD (Fig. 4).

The majority of the ND-fibre grains have spatially-uncorrelated misorientation axis distributions with strong maxima occurring nearer to the ND than the RD or TD and a significant proportion of these maxima are located very close to the ND (**Figs. 8** and **9**). This indicates that the overall orientational spread of an ND-fibre grain is more likely to be concentrated about the ND than concentrated about another axis or randomly distributed. Thus, a higher proportion of ND-fibre grains belong to Type B (Fig. 5(b)) than Types A (Fig. 5(a)) or C (Fig. 5(c)) when classified according to their overall orientational spread. The spatially-correlated misorientation axis distributions (**Figs. 10** and **11**) indicate that short-range orientational variation generally does not involve rotation about the ND. The misorientation axes for spatially-correlated misorientations are mostly located in or near the TD–ND plane, but are concentrated nearer to the TD than the ND. It may be noted that the spatially-correlated misorientation axis distributions presented

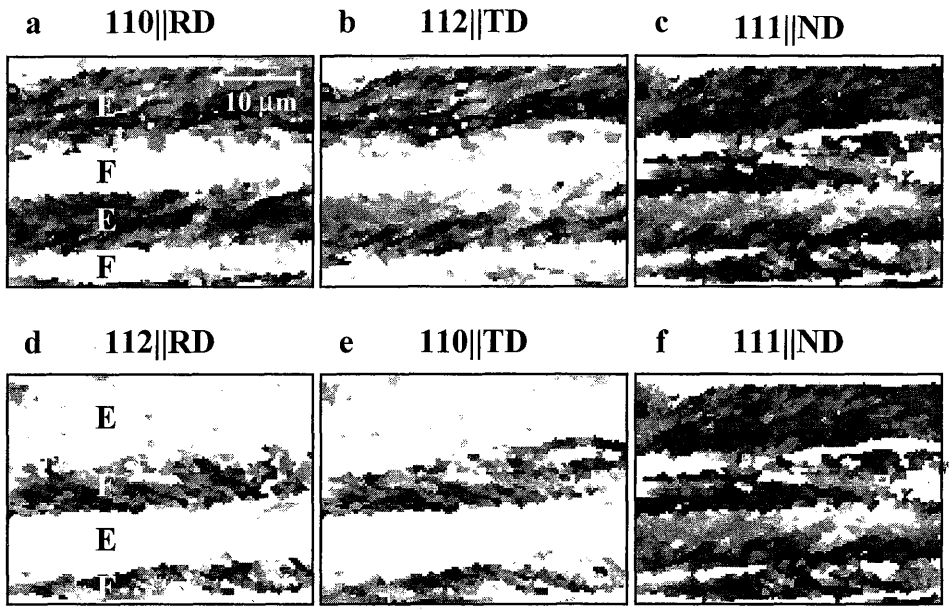

Fig. 6. Images of orientational change in four ND-fibre grains (two grains of E: {111}⟨110⟩ orientation and two grains of F: {111}⟨112⟩orientation) on the RD–ND section. The maps have been shaded to show rotation away from the ideal orientation about three mutually perpendicular axes (*i.e.* rotation away from each of the three orientational fibres that intersect at the relevant ideal orientation). In each image, the grey-scale runs from black on the nominated ideal fibre to white 15° or more away from the ideal fibre.

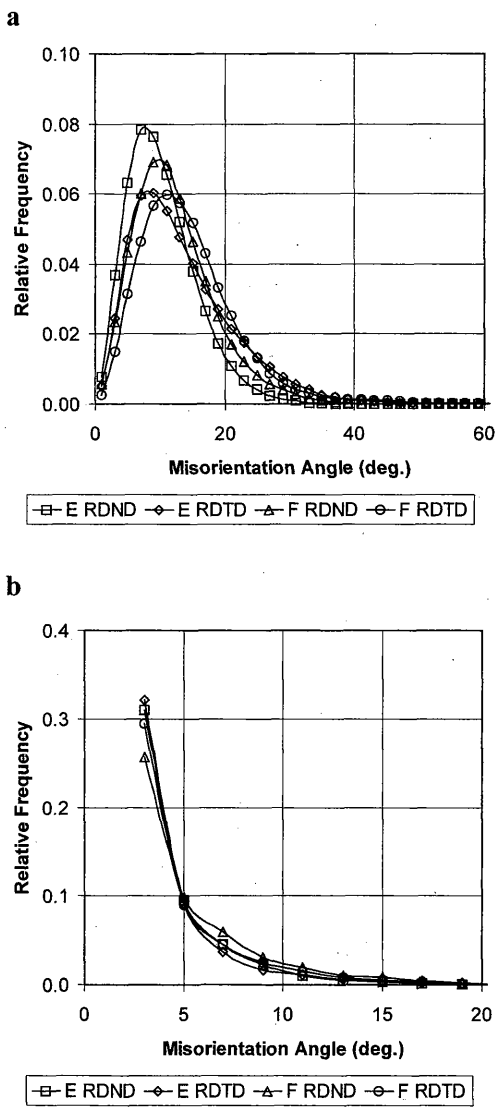

Fig. 7. Frequency *vs.* misorientation angle distributions for (a) spatially uncorrelated and (b) spatially correlated misorientations in ND-fibre grains (E: {111}⟨110⟩ and F: {111}⟨112⟩) appearing in RD–ND and RD–TD sections. Each curve represents the average of the misorientation angle distributions of four grains.

in Figs. 10 and 11 are for an angular range of 2–8°. These distributions were plotted for a number of different angular ranges for all sixteen grains and the general shape of the distribution on the pole figure was similar regardless of the angular range chosen, as long as the number of misorientations within the angular range was sufficiently large. An example for one grain is shown in **Fig. 12**.

Misorientation axis distributions were examined for all sixteen ND-fibre grains with respect to the crystal coordinate system as well as the sample coordinate system (see **Fig. 13** for selected examples). The intensities are much weaker with respect to the crystal coordinate system than the sample coordinate system, although the intensities appearing on inverse pole figures and pole figures are not directly comparable. (For instance, if rotation is occurring consistently about the ⟨111⟩||ND axis, it is not occurring about the other ⟨111⟩ axes, and the intensity plotted at the ⟨111⟩ node of the inverse pole figure is weakened as a result.) In cases where the spatially-uncorrelated misorientation axis distribution shows a maxima very near to ND when plotted in the sample coordinate system, the same distribution shows a maxima near ⟨111⟩ when plotted in the crystal coordinate system (Fig. 13(a)), as might be expected. However, in cases where the maxima is displaced significantly from ND in the sample coordinate system, ⟨111⟩ rotation is only slightly favoured (Fig. 13(b)), or not favoured at all (Fig. 13(c)). More than half the spatially-correlated distributions have maxima near ⟨110⟩ relative to the crystal coordinate system and the favouring of the ⟨110⟩ axis is particularly strong for F grains whose distributions have maxima very near TD relative to the sample coordinate system (Fig. 13(d)), as might be expected since these grains have ⟨110⟩||TD. However, it is notable that the favouring of a ⟨110⟩ rotation axis also occurs in several E grains (for example, Fig. 13(e), 13(f)) and for these grains the maxima with respect to the sample coordinate system tends to be rotated towards the ND from the TD.

4. Discussion

The general microstructural characteristics of RD-fibre and ND-fibre grains identified in this work are consistent with previous studies, reviewed by Hutchinson,[14] showing that RD-grains deform relatively homogeneously, while

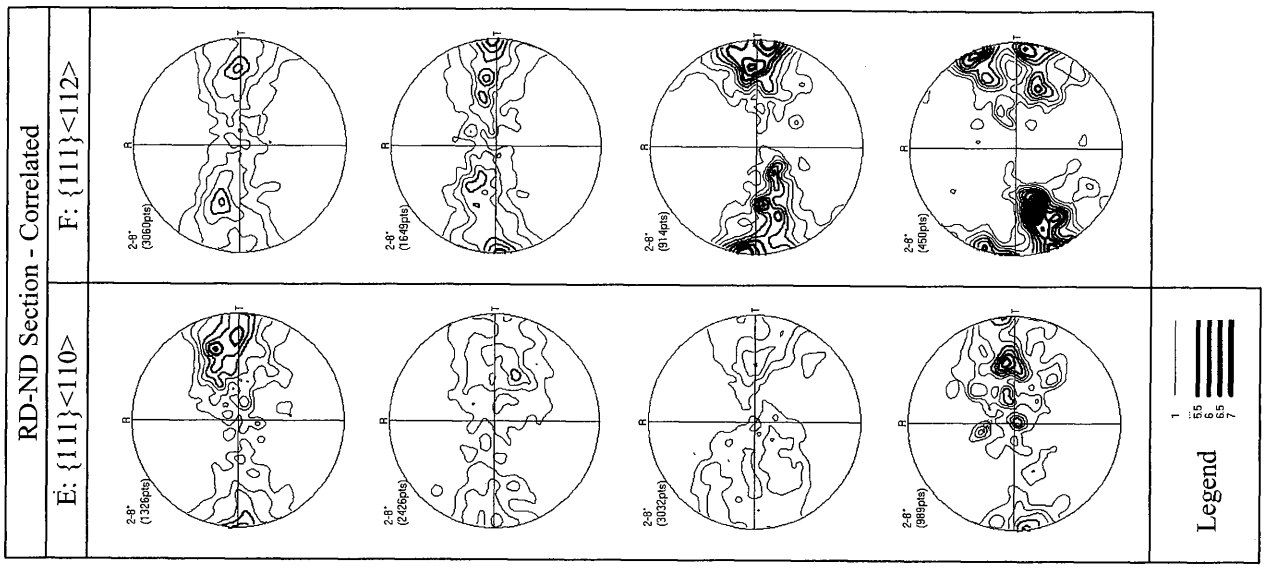

Fig. 10. Distribution of spatially-correlated misorientation axes for eight ND-fibre grains (RD–ND section).

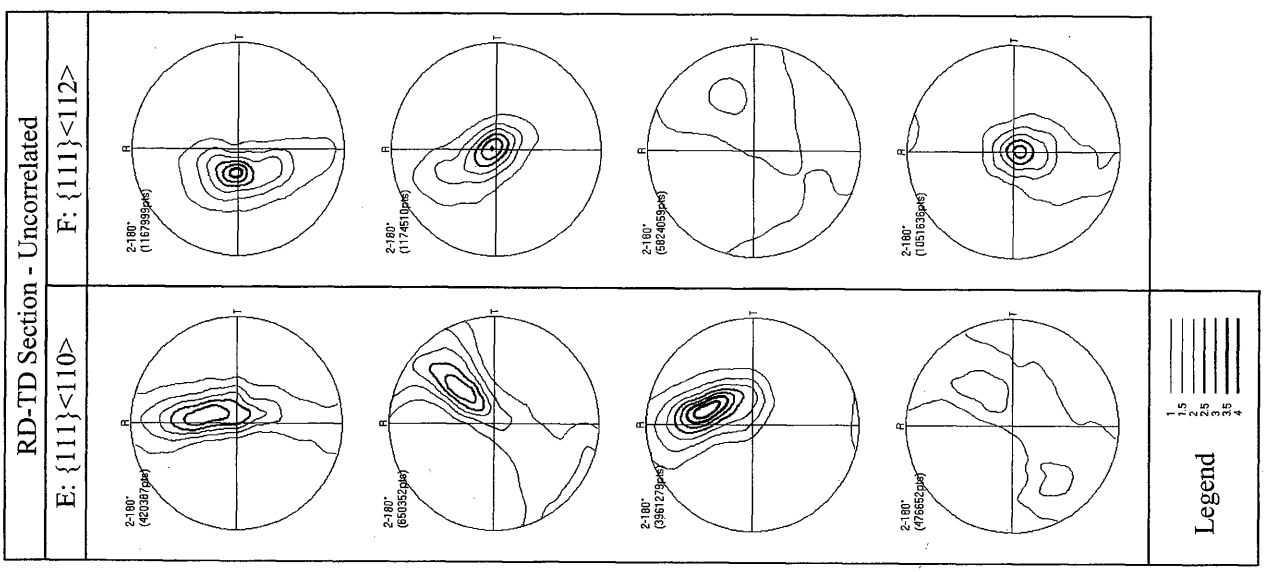

Fig. 9. Distribution of spatially-uncorrelated misorientation axes for eight ND-fibre grains (RD–TD section).

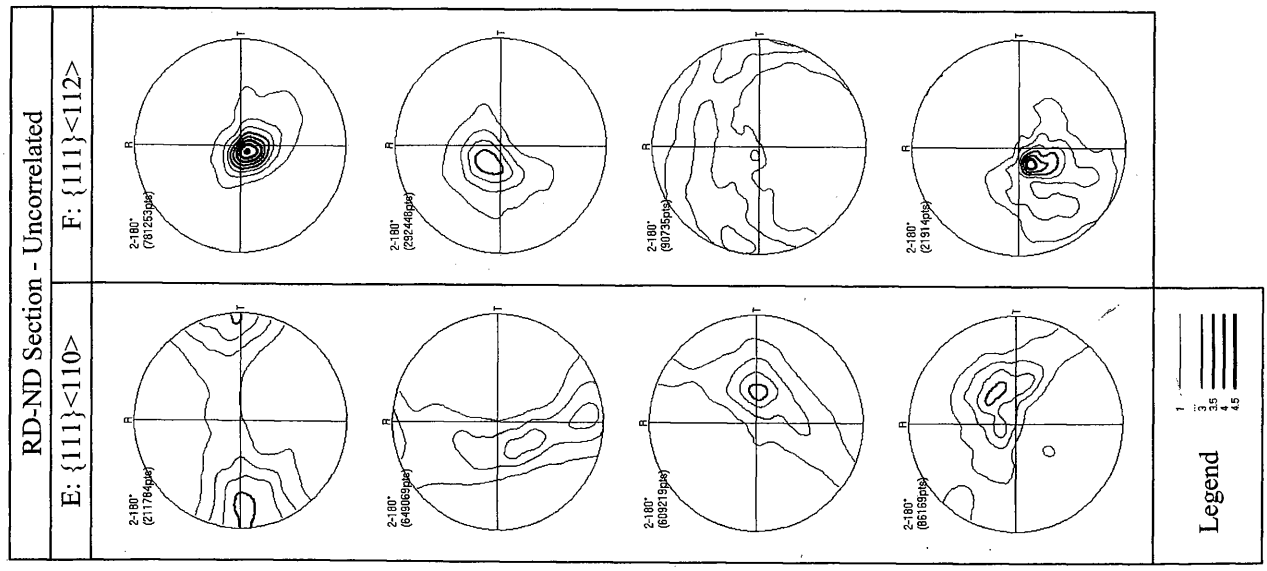

Fig. 8. Distribution of spatially-uncorrelated misorientation axes for eight ND-fibre grains (RD–ND section).

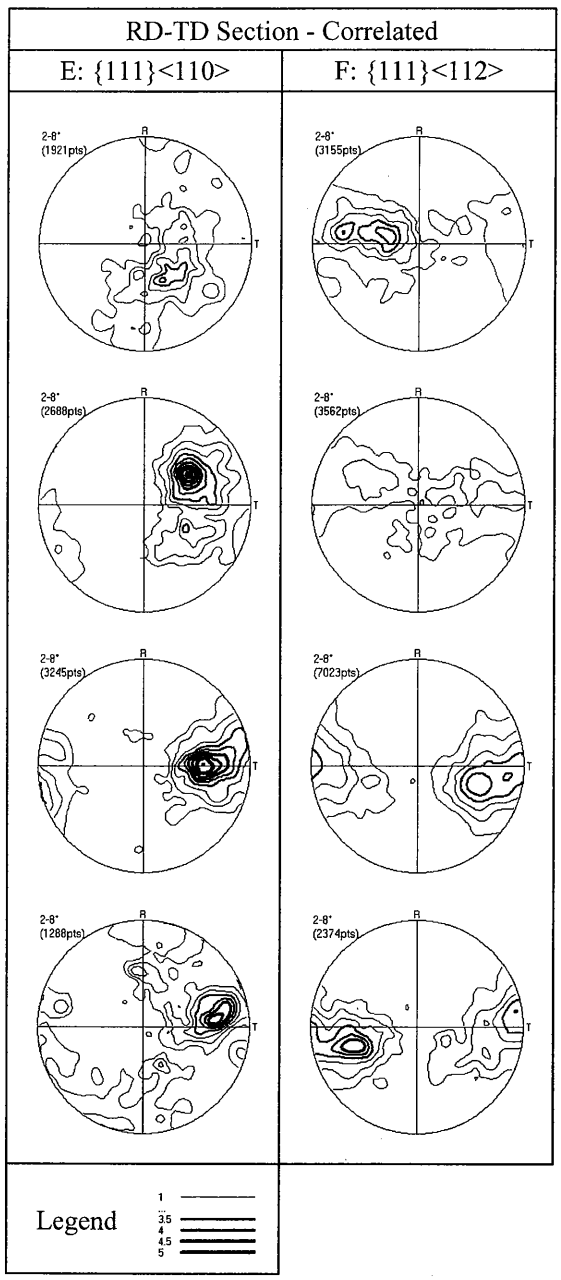

Fig. 11. Distribution of spatially-correlated misorientation axes for eight ND-fibre grains (RD–TD section).

ND-grains are often marked by bands at angles of approximately 20 to 35° to the RD in the RD–ND plane. The difference between RD-grains and ND-grains with respect to their degree of deformation (mean thickness in the ND of 3.5 μm for RD-grains and 6.8 μm for ND-grains) contrasts with work by Samajdar *et al.*[13], which found RD-fibre and ND-fibre grains in cold-rolled ultra-low-carbon (ULC) steel to have similar average thicknesses in the ND for reductions between 50 and 90%. However, the higher degree of deformation of RD-fibre grains compared with ND-fibre grains is consistent with previous suggestions of a correspondence with Taylor factor,[14,17] discussed further below.

The significantly higher average misorientation for ND-fibre grains than RD-fibre grains (Fig. 4) is consistent with point-to-point orientation profiles measured using EBSD on {112}⟨110⟩ and {554}⟨225⟩ grains in a 70% cold-rolled ULC steel,[27] as well as TEM measurements of misorientations between neighbouring cells in H, I, E and F regions in a 90% cold-rolled IF steel.[3] It is also consistent with measurements of the stored energy of deformation, which show an increase with progression along the RD-fibre from {100}⟨110⟩ through {111}⟨110⟩ to {110}⟨110⟩.[14] However, it contrasts with an investigation on a 60% cold-rolled ULC steel,[28] which did not find a significant difference between the average misorientation in RD-fibre and ND-fibre grains. Although the investigation on the less heavily rolled material[28] was based on a relatively small number of grains (four RD-grains and four ND-grains), this may indicate that a significant difference in the short-range orientational variation present in RD-fibre and ND-fibre grains only develops at higher rolling reductions.

The differences in the behaviours of RD-grains and ND-grains in terms of overall deformation and localisation of deformation (banding) can be rationalised in terms of the variation in Taylor factor with orientation, along the lines used by Vanderschueren *et al.*[17] and Hutchinson.[14] RD-grains (H and I orientations) have relatively low Taylor factors, while ND-grains (E and F orientations) have higher Taylor factors and the Taylor factor of the J orientation is even higher.[29] Grains with low Taylor factors require less shear strain (summed over all active slip systems) to accommodate a given amount of deformation, while those with higher Taylor factors require more shear strain. Consequently, low Taylor factor grains can accommodate slip more easily and absorb a larger proportion of the overall sample deformation, while grains with higher Taylor factors work-harden more rapidly and resist further defor-

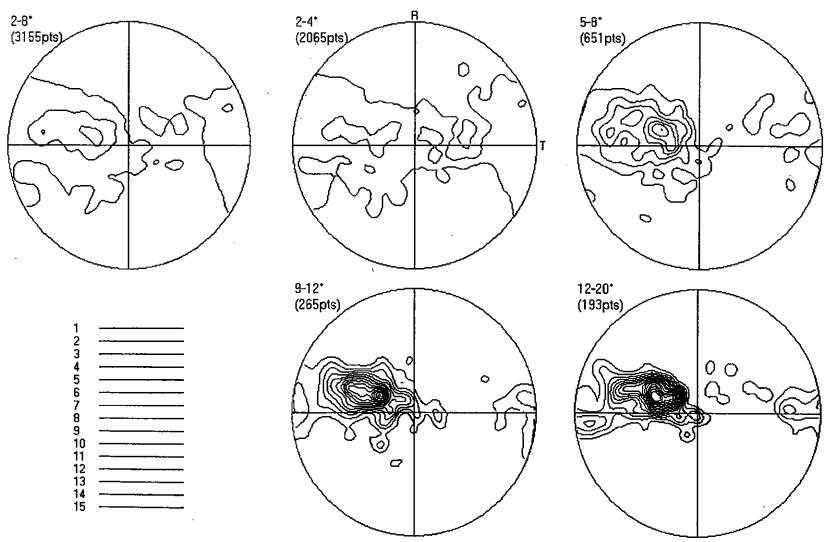

Fig. 12. Spatially-correlated misorientation axis distributions, using different misorientation angle ranges, for one grain of F: {111}⟨112⟩ orientation on the RD–TD section.

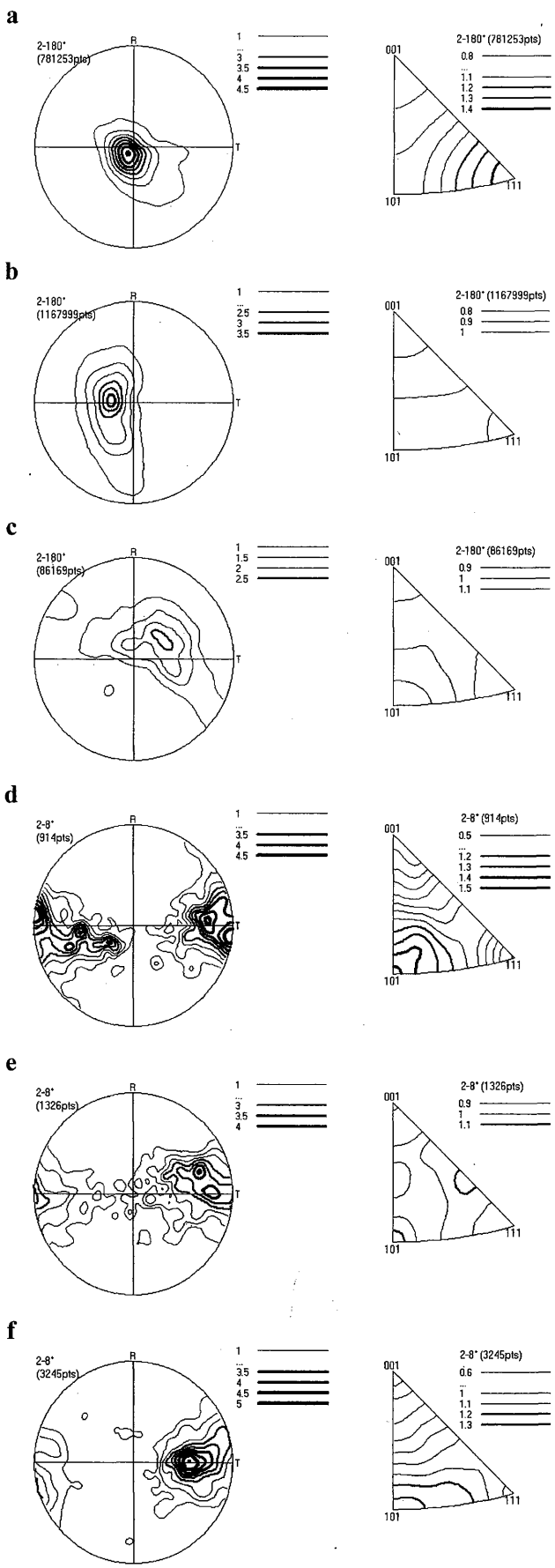

Fig. 13. Misorientation axis distributions for selected ND-fibre grains with respect to both sample and crystal coordinate systems: (a)–(c) spatially-uncorrelated, (d)–(f) spatially-correlated.

mation to a greater extent. Hence, RD-grains deform considerably more than ND-grains and J-oriented grains deform the least, as seen in Fig. 2. It is interesting, however, that H and I grains were found to have the same mean thickness, despite a difference in their Taylor factors. The much higher degree of banding in ND-grains (and grains of J orientation) compared with RD-grains may be rationalized, at least qualitatively, by reference to the difference in Taylor factors: localisation of slip is more likely to cause a significant reduction in the energy required for deformation in a grain with a high Taylor factor than in a grain with a low Taylor factor.[14]

The preference for rotations about the ND in the long-range (spatially-uncorrelated) orientational spreads of ND-fibre grains (Figs. 8 and 9) is consistent with many previous observations of ND-rotation within ND-fibre grains.[6,21,22] In an attempt to explain these observations, Inagaki[21] has focused on grain boundary effects and Duggan and co-workers[6,22] have emphasised large scale deformation banding. However, it is also known that in-grain shear bands play an important role in the formation of high misorientations within ND-fibre grains.[4,30] Crystal plasticity studies of shear bands[4,20] and simple shear deformation[31] have shown that, in the main, the preferred crystal rotation is around an axis perpendicular to both the shear plane normal and the shear direction. In rolling, this axis corresponds with the transverse direction. Consequently, material within a shear band is expected to be rotated predominantly around an axis close to the TD in relation to the adjacent matrix. A case in point is the generation of Goss textures in shear bands within $\{111\}\langle 112\rangle$ grains.[18]

Hutchinson and Bate[32] have shown that ND rotations as a result of shear banding can be rationalized using the following two assumptions. (1) During (homogeneous) rolling deformation the general rotation trend is towards,[33] and then along,[32] the ND fibre. (2) In-grain shear bands exist only for a limited time (strain).[4,18,34] When a shear band forms in an ND-fibre grain, the rotations in the band are likely to be around the TD while that of the adjacent material is likely to be around the ND. Once the band has exhausted itself, the material in the band will tend to rotate back towards the ND fibre, arriving at a different location on the fibre to that of the adjacent material. In this manner, rotations about an axis near the ND can be expected to arise.

According to this argument, the actual misorientation axes present between adjacent volumes at a given time will span the range from the TD to the ND depending on the relative rotations occurring in the bands and in the adjacent material. This will be a function of orientation and shear band strain. One of the important findings presented in this paper is that the short-range (spatially-correlated) orientational variation in ND-fibre grains (Figs. 10 and 11) does indeed show a preference for rotation about axes lying between the TD and the ND, but closer to the TD. When misorientations over a distance spanning a number shear bands are considered, one would expect the local effects (*i.e.* TD rotations) to become less prominent. Consequently, ND rotations dominate longer range misorientations, which is consistent with the spatially-uncorrelated data in Figs. 8 and 9. While this mechanism provides a plausible explanation for the most common distributions of misorientation axes found in ND-fibre grains, other mechanisms (such as deformation banding in response to the constraints of neighbouring grains) also contribute to their fragmentation.

During recrystallization of an IF steel, nucleation occurs

predominantly in ND-fibre grains and the growing nuclei consume their parent grain and neighbouring ND-fibre grains before progressing into RD-fibre grains.[14,25] Quantification of the degree and nature of short-range orientational variation in ND-fibre grains is important for the development of models of oriented nucleation. Quantification of long-range orientational variation within ND-fibre grains is important for modelling the early to intermediate stages of growth. However, attempts to incorporate the spatial variation of orientation into recrystallization models are still in their early stages. For example, Réglé *et al.*[35] have developed a model that assumes initial growth of differently-oriented nuclei into their deformed parent (ND-fibre) grains, before subsequent growth into surrounding grains. The orientation of an intragranular nucleus is randomly chosen within 7.5° of the orientation of the parent grain, while the orientation of an intergranular nucleus is randomly chosen between the two different orientations of the parent grain given by full constraints and relaxed constraints Taylor simulations.[35] The results in the present paper have demonstrated that short-range orientational variation in ND-fibre grains is not random, but occurs preferentially about certain rotation axes (those lying approximately in the TD–ND plane and nearer to the TD than the ND). These results could be used to modify the distribution of orientations from which recrystallization models choose the orientations of intragranular nuclei and possibly also intergranular nuclei (although the misorientation angle distributions for regions near grain boundaries have not yet been investigated as a separate case). As the models become more sophisticated, they may also be modified to simulate initial growth of recrystallization nuclei into parent grains having significant long-range orientational spreads (*e.g.* Fig. 7(a)) about a representative distribution of axes (Figs. 8 and 9).

5. Conclusions

The analyses of microstructure and microtexture presented in this paper lead to the following conclusions regarding orientational variation in the deformed microstructure of cold-rolled interstitial-free steels.

(1) Regions belonging to the ND-fibre, from near-{111}⟨110⟩ to near-{111}⟨112⟩, are heavily-banded and exhibit a high degree of short-range orientational variation associated with the bands.

(2) Regions belonging to the partial RD-fibre, from near-{001}⟨110⟩ to near-{112}⟨110⟩, are not heavily banded and exhibit much smaller short-range orientational variation.

(3) At a rolling reduction of 75%, RD-fibre grains are reduced to approximately half the thickness (parallel to the ND) of ND-fibre grains.

(4) The differences in thickness reduction and degree of banding between RD-fibre regions and ND-fibre regions are consistent with expectations based on differences in Taylor factor.

(5) The overall orientational spread in ND-fibre grains commonly involves rotation about the sample normal direction (which also corresponds approximately to rotation about a ⟨111⟩ crystallographic axis, given the approximate ⟨111⟩||ND orientation of the grains).

(6) Short-range orientational variation in ND-fibre grains is characterised by rotations about axes within 15° of the TD–ND plane and having inclinations of between 0° and 50° to the TD. This is associated with a tendency towards rotation about the ⟨110⟩ axis in a significant proportion of the grains.

Acknowledgement

The authors would like to acknowledge the Australian Research Council (ARC) for funding this work.

REFERENCES

1) R. K. Ray, J. J. Jonas and R. E. Hook: *Int. Mater. Rev.*, **39** (1994), 129.
2) L. Kestens and J. J. Jonas: *ISIJ Int.*, **37** (1997), 807.
3) I. Samajdar, B. Verlinden, P. Van Houtte and D. Vanderschueren: *Mater. Sci. Eng.*, **A238** (1997), 343.
4) M. R. Barnett: *ISIJ Int.*, **38** (1998), 78.
5) M. R. Barnett and L. Kestens: *ISIJ Int.*, **39** (1999), 923.
6) B. J. Duggan, G. L. Liu and Y. Y. Tse: Proc. of 4th Int. Conf. on Recrystallization and Related Phenomena, ed. by T. Sakai and H. G. Suzuki, The Japan Institute of Metals, Sendai, (1999), 367.
7) L. Kestens, N. Yoshinaga, D. Vanderschueren and B. C. De Cooman: Proc. of 4th Int. Conf. on Recrystallization and Related Phenomena, ed. by T. Sakai and H. G. Suzuki, The Japan Institute of Metals, Sendai, (1999), 745.
8) L. Kestens and J. J. Jonas: *Met. Mater.*, **5** (1999), 419.
9) L. Kestens and Y. Houbaert: Proc. of 21st Risø Int. Symp. on Materials Science: Recrystallization—Fundamental Aspects and Relations to Deformation Microstructure, ed. by N. Hansen *et al.*, Risø National Laboratory, Roskilde, Denmark, (2000), 379.
10) J. J. Jonas and L. Kestens: Proc. of 1st Joint Int. Conf. on Recrystallization and Grain Growth, ed. by G. Gottstein and D. A. Molodov, Springer-Verlag, (2001), 49.
11) H. Magnusson, D. Juul Jensen and B. Hutchinson: *Scr. Mater.*, **44** (2001), 435.
12) I. Samajdar, B. Verlinden and P. Van Houtte: *Acta Mater.*, **46** (1998), 2751.
13) I. Samajdar, B. Verlinden, L. Kestens and P. Van Houtte: *Acta Mater.*, **47** (1999), 55.
14) B. Hutchinson: *Philos. Trans. R. Soc. (London) A*, **357** (1999), 1471.
15) V. M. Nandedkar, I. Samajdar and K. Narasimhan: *ISIJ Int.*, **41** (2001), 1517.
16) W. B. Hutchinson: *Acta Metall.*, **37** (1989), 1047.
17) D. Vanderschueren, N. Yoshinaga and K. Koyama: *ISIJ Int.*, **36** (1996), 1046.
18) M. D. Nave and M. R. Barnett: *Mater. Sci. Forum*, **408–412** (2002), 907.
19) H. Inagaki: *Z. Metallkd.*, **78** (1987), 431.
20) K. Ushioda and W. B. Hutchinson: *ISIJ Int.*, **29** (1989), 862.
21) H. Inagaki: *Trans. Jpn. Inst. Met.*, **28** (1987), 251.
22) Y. Y. Tse, G. L. Liu and B. J. Duggan: *Scr. Mater.*, **42** (2000), 25.
23) Q. Liu, B. L. Li, W. Liu and X. Huang: Proc. of 21st Risø Int. Symp. on Materials Science: Recrystallization—Fundamental Aspects and Relations to Deformation Microstructure, ed. by N. Hansen *et al.*, Risø National Laboratory, Roskilde, Denmark, (2000), 423.
24) P. Gangli, L. Kestens and J. J. Jonas: *Metall. Mater. Trans. A.*, **27A** (1996), 2178.
25) E. Lindh, B. Hutchinson and P. Bate: *Mater. Sci. Forum*, **157–162**, (1994), 997.
26) R. S. Witte and J. S. Witte: Statistics, 5th ed., Harcourt Brace College Publishers, Forth Worth, (1997).
27) L. Kestens, K. Verbeken and J. J. Jonas: "The Role of Strain Heterogenetics in the Formation of Annealing Textures in Ultra-low Carbon Steels," *Phys. Met. Metallogr.*, in press.
28) K. Verbeken and L. Kestens: *Mater. Sci. Forum*, **408–412**, (2002), 559.
29) J. J. Jonas and L. Kestens: *Mater. Sci. Forum*, **204–206**, (1996), 155.
30) H. Ning, B. J. Duggan, G. L. Liu and L. X. Zhang: Proc. of 11th Int. Conf. on Textures of Materials—ICOTOM 11, International Academic Publishers, Beijing, (1996), 525.
31) M. R. Barnett and F. Montheillet: *Acta Mater.*, **50** (2002), 2285.
32) B. Hutchinson and P. Bate: Proc. of IF Steels 2003, ISIJ, Tokyo, (2003), 337.
33) J. J. Jonas, L. Kestens and A. O. Humphreys: Proc. of IF Steels 2003, ISIJ, Tokyo, (2003), 393.
34) B. J. Duggan, M. Hatherly, W. B. Hutchinson and P. T. Wakefield: *Met. Sci.*, **12** (1978), 343.
35) H. Réglé, D. Grandemange, A. Miroux and B. Bacroix: *Mater. Sci. Forum*, **408–412** (2002), 451.